


Effective fluorine removal using mixed matrix membrane based on polysulfone: adsorption performance and diffusion behavior

Xinbo Zhang^{a,b}, Guoyi Sui^{a,b}, Zhe Wang ^{a,b,*}, Huu Hao Ngo^{a,c}, Wenshan Guo^{a,c}, Haitao Wen^{a,b}, Dan Zhang^{a,b}, Xiao Wang^d and Jianqing Zhang^d

^a Joint Research Centre for Protective Infrastructure Technology and Environmental Green Bioprocess, Department of Environmental and Municipal Engineering, Tianjin Chengjian University, Tianjin 300384, China

^b Tianjin Key Laboratory of Aquatic Science and Technology, Tianjin Chengjian University, Jinjing Road 26, Tianjin 300384, China

^c Centre for Technology in Water and Wastewater, School of Civil and Environmental Engineering, University of Technology Sydney, Sydney, NSW 2007, Australia

^d TG Hilyte Environment Technology (Beijing) Co., LTD., Beijing 100000, China

*Corresponding author. E-mail: wz19860101@126.com

 ZW, 0000-0001-9573-4258

ABSTRACT

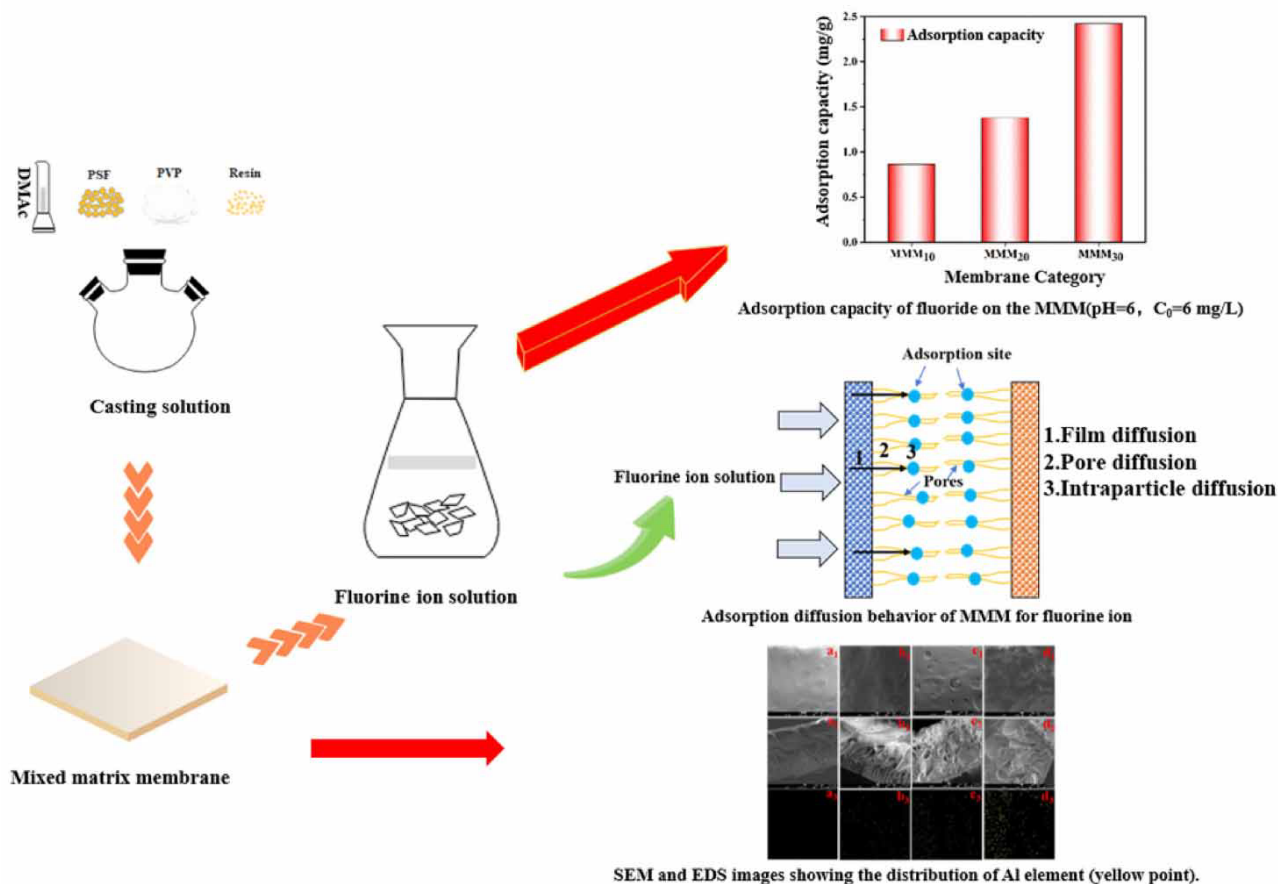
Fluorine is one of the essential trace elements for human life activities, but excessive intake of fluoride poses a great risk to people's health. In this paper, a series of mixed matrix membrane (MMM)-based polysulfone for removing fluoride were prepared by phase inversion, and their properties, adsorption capacity, adsorption isotherms, adsorption kinetics of fluoride ions, and mechanism were all investigated. The results confirmed that the MMM contained a large number of hydroxyl and aluminum functional groups due to resin being added. The MMM exhibited the best fluorine ion adsorption capacity of 2.502 mg/g at a pH of 6 with the initial concentration of 6 mg/L. As well, adsorption kinetics of fluorine ion on MMM followed the pseudo-second-order model, while the adsorption behavior of fluorine ion on MMM was well simulated by the Langmuir isotherm model. The adsorption capacity of MMM remained stable after six cycles and the regeneration efficiency was still above 80%, resulting in a long-term stability adequate for fluorine ion removal. Complexation and ion exchange played a key role in the fluorine ion adsorption of MMM. These results indicated the MMM as novel type of absorbent had an excellent capacity for removing fluoride.

Key words: absorbent, adsorption, fluoride removal, mixed matrix membrane, novel, resin

HIGHLIGHTS

- MMM was prepared via phase inversion for removing fluoride.
- The addition of resin significantly enhanced fluoride removal via the membrane.
- The MMM exhibited the maximum fluoride adsorption capacity of 2.502 mg/g.
- Fluoride adsorption by MMM depended on ion-exchange and complexation.
- MMM retained stable fluoride adsorption capacity after six cycles.

GRAPHICAL ABSTRACT



INTRODUCTION

Fluoride is a persistent and non-degradable substance that is toxic to humans, flora and fauna. Fluoride is involved in gene expression, cell cycle, ion transport, and oxidative stress (Barbier *et al.* 2010), which can even induce neuronal degeneration and other dangerous outcomes (Cao *et al.* 2013). Fluoride is also essential to the human body because a small amount of fluoride uptake can prevent cavities. However, excessive fluoride existing in water can cause various diseases such as rickets, neurological disorders, osteoporosis, arthritis, fragile bones, and fluorosis (Dong & Wang 2016). Fluoride is also one of the groundwater contaminants classified by the World Health Organization (WHO) that should have a maximum concentration of 1.5 mg/L (Grabow *et al.* 2001). The fluoride contamination of groundwater is due to the dissolution of naturally fluoride-rich minerals, on one hand. On the other hand, artificial fluoride pollution is a consequence of factories' generation of wastewater, which is common for the metal refining, plating, semiconductor industries, which are just a few examples. Hence, the preparation of a novel and efficient absorbent to reduce the permissible limit of fluoride concentration has been an urgent issue in recent years.

There are at present many methods reported to remove fluoride from water, such as precipitation separation, electrocoagulation, adsorption, ion exchange, and membrane separation. The precipitation separation method, widely used for removing fluoride in high concentrations from traditional industries, has the advantages of convenient operation and low cost. However, it is difficult to effectively remove fluoride with a concentration of below 5 mg/L, because the chemical precipitation process is constrained by the solubility of the formed salt. Additionally, precipitation separation could cause secondary pollution such as aluminum sludge with high water content. Therefore, what is needed is a way to improve the costs involved before dehydration and drying treatment (Paudyal *et al.* 2012). Electrocoagulation has the advantages of

relative simplicity and small footprint, but the electrode surface is prone to passivation during the treatment process (Emam-jomeh & Sivakumar 2009).

Among the commonly used fluoride removal treatment technologies, the adsorption method is highly efficient, simple to use and low cost. The removal of fluoride by adsorption of adsorbent materials is the most advantageous in terms of operating costs and ease of operation (Wendimu *et al.* 2017). Several adsorbents have been extensively explored, such as ion exchange resin, aluminum modified iron oxides, and synthesis of hydroxyapatite. Currently, the resin has been widely used due to its good stability, adsorptive capacity and adaptability (Sarici-Özdemir & Önal 2010). Membrane separation has a selective separation function. Reverse osmosis (RO) and nanofiltration (NF) have been used for fluoride removal, and they both have the advantages of good interception performance, stability, and simple operational processes. However, these membrane processes consume a lot of energy and take up a lot of investment dollars. It is difficult to reject fluoride by the size exclusion in the membrane separation process. For example, microfiltration and ultrafiltration membranes haven't the ability to remove fluorine. Nanofiltration membrane can partially remove fluorine ions with fluorine removal rate of about 50% (Owusu-Agyeman *et al.* 2018). Therefore, it is inefficient for fluoride removal directly by membrane filtration. As a consequence, substances or functional groups with fluoride removal function, such as resins, nanoparticles, and hydroxyl groups, are introduced into membrane materials, which can enhance fluoride removal. Based on this, the use of mixed matrix membranes (MMMs) is proposed. For MMMs, adsorbent materials can be doped in polymer matrix to develop selective separation properties of adsorption and filtration of membranes. Thus, not only fluoride removal but also further removal of suspended matter, microorganisms, etc. can be achieved. Combining adsorption and membrane separation indicates better defluorination ability and minimizes secondary pollution, while improving the membrane material's efficient, economical, convenient, and stable fluoride removal.

Polymer blends have already found applications in numerous fields, such as organic electronics, optics, biotechnology and membrane technology. Mean-field theory can be used to explain the copolymerization effect in polymer blends (Rana *et al.* 2000). In the mean-field regime the Flory–Huggins interaction parameter is used to evaluate the interaction between the polymer and the solvent, and the magnitude of its value reflects the strength of the solvent–solvent interaction to be measured (Janssen *et al.* 1993). In the course of systematic studies of polymer blending systems, one of the miscible blending systems is the polysulfone (PSF)-chelating type ion exchange resins with cross-linked polystyrene (PS) copolymer system.

Polymer fluoride removal resin was introduced into the polysulfone casting solution to prepare the MMM via phase inversion for removing fluoride ions. Due to the polymeric resin in the pore hindering the transport diffusion (Guillen *et al.* 2011), the polymer resin needs to be ground into fine particles so that they are evenly distributed in the mesoporous walls of the membrane matrix and provide more selective ligands (Zhao *et al.* 2011). Due to the better flexibility of the organic resin, the resin is compatible with the polymer matrix in the formation of MMMs. Additionally, the resin is not easy to lose after the formation of MMM owing to good adhesion between the polymer matrix and the filler; thus the MMM formed has good stability.

In this work, surface functional groups and morphology of the prepared MMM were characterized by Fourier transform infrared (FTIR) and Scanning electron microscopy (SEM). Furthermore, the fluoride ion adsorption capacity of MMM was investigated. Meantime, the effects of pH, co-existing anions, and defluorination resin dosage on the adsorption of fluoride ions were evaluated. In the meantime, the mechanism of fluoride removal from water by MMM was explored.

MATERIALS AND METHODS

Materials

Tulsion[®] CH-87 is a moist spherical bead resin (containing aluminum groups) with the particle size range of 0.3–1.2 mm purchased from Beijing Kehaisi Technology Company, China. The resin was crushed by high speed multi-function pulverizer (SL-100, purchased from a Songqing hardware factory, Zhejiang Yongkang, China) and screened out of the 200 mesh sieves. N, N-dimethylacetamide (DMAC), Polysulfone (PSF) (P-3500 LCD, Mw = 75,000–81,000 g/mol) was purchased from Solvay, USA. Polyvinylpyrrolidone (PVP), NaF and the other reagents used in the experiments were obtained by Tianjin Damao Chemical Reagent Factory. All of them are of analytical grade. Sodium hydroxide and hydrochloric acid solution (0.1 mol/L) were employed to adjust the pH. Deionized (DI) water (18.2 MΩ cm at 25 °C) was obtained from a Millipore Direct-Q UV water purification system.

MMM preparation

MMM was prepared by the phase inversion (Shi *et al.* 2013). Firstly, PSF (17 g) and the pore-forming agent of PVP (8 g) were slowly and uniformly added into 75 mL of DMAC at 80 °C, and then the Tulsion CH-87 resin was added to the mixed solution and stirred continuously for 8 h to prepare the casting solution. The resin dosages were 0 g, 10 g, 20 g, and 30 g, respectively, and subsequently, the casting solution was degassed by standing and cooled down to room temperature. Then the casting solution was poured onto a clean and flat glass surface, scraped evenly to make MMM of uniform thickness, and next the glass plate was immersed in the coagulation bath (DI water) at 25 °C to obtain the MMM. It was finally washed with DI water to remove residual solvent and impurity, and then stored in ultrapure water for back-up. The prepared MMMs were tagged PSF, MMM₁₀, MMM₂₀, and MMM₃₀, which corresponded to the resin dosages of 0 g, 10 g, 20 g, and 30 g, respectively.

Characterization and analysis

FTIR (Nicolet iS10, United States of America) was used to characterize the membrane surfaces of PSF, MMM₁₀, MMM₂₀, and MMM₃₀ with the adsorption spectrogram in the 500–4,000 cm⁻¹ range and recorded. At the same time, the morphology and elements contained in MMM were characterized. The cross-section and surface of the membrane were observed by SEM (JSM-7800F, Japan) and the elements contained in the MMM surface were determined by energy-dispersive spectrometry (EDS). Ion concentration was measured via ion chromatography (Dionex Aquion, Thermo Scientific, United States).

Adsorption experiments

Before the adsorption experiment, the MMM samples were dried and weighed, and cut a sample of a certain size for use (PSF has no fluoride removal capability). MMM was put into a conical flask containing 200 mL of fluorine ion solution, and then the flask was sealed and continuously shaken with a shaker at 100 rpm at 25 °C for 8 h. At the end of the experiment the supernatant was taken to determine its properties. The supernatant was filtered through a 0.45 µm microporous membrane. The adsorption capacity was calculated from the following equations:

$$q_e = \frac{(C_0 - C_e)V}{m} \quad (1)$$

where C_0 (mg/L) and C_e (mg/L) are the initial and final equilibrium concentrations of fluorine ion, V (L) denotes the volume of solution, and m (g) stands for the mass of the adsorbent.

The adsorption isotherms were selected for MMM₁₀, MMM₂₀, MMM₃₀ samples that were part of the adsorption experiments. First, the dried and weighed MMM samples were shaken with fluorine ion solutions of 5–160 mg/L concentration in a shaker at 100 rpm and 25 °C for 8 h, the supernatant was filtered through a 0.45 µm microporous membrane. Once this was done the supernatant was taken for analysis. The equation of the Langmuir isotherm model is documented immediately below:

$$\text{Langmuir model: } q_e = \frac{q_m b C_e}{1 + b C_e} \quad (2)$$

where q_e represents the adsorption capacity at equilibrium, C_e is the concentration of fluorine ion at equilibrium, q_m is the maximum adsorption capacity, and b is the sorption coefficient of Langmuir (L/mg).

The Freundlich isotherm model is written here:

$$\text{Freundlich model: } q_e = K_F C_e^{1/n} \quad (3)$$

where n is the characteristic constant used to characterize the adsorption strength, K_F (mg/g) is Freundlich adsorption constant.

$$\text{Redlich–Peterson model: } q_e = AC_e / (1 + BC_e^g) \quad (4)$$

where q_e represents the adsorption capacity at equilibrium, C_e is the concentration of fluorine ion at equilibrium, A , B are Redlich–Peterson parameters, and g is Redlich–Peterson constant, lying between 0 and 1.

$$\text{Dubinin–Radushkevich (D-R): } q_e = q_{\text{DR}} \exp \left\{ -\beta \left[\text{RT} \ln \left(1 + \frac{1}{C_e} \right) \right]^2 \right\} \quad (5)$$

where β ($\text{mol}^2 \cdot \text{J}^{-2}$) is the D-R isotherm constant, which is the mean sorption energy coefficient. R and T indicate a constant related to adsorption energy, gas constant ($8.314 \text{ J} \cdot \text{mol}^{-1} \cdot \text{K}^{-1}$) and temperature (K), respectively. The mean adsorption free energy E ($\text{kJ} \cdot \text{mol}^{-1}$) could be calculated from D-R isotherm constant β using Equation (5).

$$E = \frac{1}{(2\beta)^{1/2}} \quad (6)$$

The value of E could be used to judge the action type of adsorption. When E was $< 8 \text{ kJ} \cdot \text{mol}^{-1}$, the adsorption was mainly caused by van der Waals force and hydrogen bond interaction. When E was between 8 and $16 \text{ kJ} \cdot \text{mol}^{-1}$, the adsorption was mainly caused by ion exchange. When E was $> 16 \text{ kJ} \cdot \text{mol}^{-1}$, the adsorption was a spontaneous chemical process (Dubinin *et al.* 1947).

To investigate the influence of adsorption time on the removal effect of fluorine ions by MMM, adsorption kinetics experiments were conducted. Fluorine ion stock solutions ($1,000 \text{ mg/L}$) were prepared by dissolving NaF in DI water. The MMM_{30} sample (0.15 g) was mixed with $1,000 \text{ mL}$ F^- solutions (6 mg/L) in a plastic tube in a shaker at 100 rpm and 25°C for 8 h ; 1 mL samples were collected quickly at $5, 10, 15, 20, 25, 30, 40, 50, 60, 70, 80, 90, 120, 150, 180, 210,$ and 240 min , and the supernatant was filtered through a $0.45 \mu\text{m}$ microporous membrane.

The MMM_{30} samples and $1,000 \text{ mL}$ of fluorine ion solution (6 mg/L) were placed in a conical flask and shaken at 100 rpm for 240 min at 25°C , and the initial pH of the solution was adjusted to 6 (optimum pH). In the time periods $5, 10, 15, 20, 25, 30, 40, 50, 60, 70, 80, 90, 120, 150, 180, 210,$ and 240 min , the supernatant was taken for the assay. In order to explain the adsorption mechanism, various kinetic models including the pseudo-first-order and pseudo-second-order models were used to fit the adsorption kinetic data.

The research of adsorption kinetics is helpful to study the chemical adsorption mechanism, which is essential to study the properties of adsorbents. Several typical kinetic models were used to analyze the experimental results (Wang *et al.* 2017).

$$\text{Pseudo-first-order model: } q_t = q_e (1 - e^{-k_1 t}) \quad (7)$$

$$\text{Pseudo-second-order model: } q_t = \frac{k_2 q_e^2 t}{1 + k_2 q_e t} \quad (8)$$

where q_e and q_t (mg/g) are the adsorption of fluorine ion at the equilibrium and at time t ; k_1 (min^{-1}), k_2 ($\text{g} \cdot \text{mg}^{-1} \cdot \text{min}^{-1}$) are the reaction rate constants of the pseudo-first-order and pseudo-second-order.

Intraparticle diffusion model:

$$q_t = k_i t^{1/2} \quad (9)$$

Film diffusion model:

$$q_t = q_e (1 - e^{-K_F t}) \quad (10)$$

Chemical reaction model:

$$q_t = q_e [1 - (1 - K_C t)^3] \quad (11)$$

where q_t (mg/g) and q_e are the adsorption of fluorine ion at time t and the equilibrium, respectively, while k_i , k_F , and k_C are the constants for the diffusion model.

Regeneration experiments

In view of the fact that the pH of 0.1 mol/L NaOH is 13, it may cause damage to the structure of the membrane. Therefore, 10% aluminum sulfate (dosing with a concentration of aluminum sulfate exceeding 10% did not produce a greater effect) was used in this experiment. Aluminum ions can replace the fluorine in the aluminum–fluorine complex to generate aluminum–fluorine precipitation, which in turn activates the aluminum-based groups in the MMM to regain adsorption capacity. At first, the membrane samples were placed into a polyethylene conical flask containing 200 mL of 6 mg/L fluoride ion solution and shaken for 8 h. The fluorine adsorption capacity q_1 was measured. Then the saturated membrane was immersed in 10% aluminum sulfate solution, which was allowed to desorb the saturated membrane for 1 h. Subsequently, the treated membrane was withdrawn and washed with excess of DI water. The amount of fluorine adsorbed q_2 was determined again. Then six consecutive experiments were performed using adsorption and desorption. The regeneration efficiency (RE) of the membrane was defined as follows:

$$RE = \frac{q_2}{q_1} \times 100\% \quad (12)$$

where q_1 and q_2 are the initial adsorption capacity of fluorine ion and the adsorption capacity after regeneration, respectively.

RESULTS AND DISCUSSION

FTIR spectra analysis

The spectra of the raw PSF and modified membrane are shown in Figure 1. The characteristic peaks of $1,151\text{ cm}^{-1}$, $1,246\text{ cm}^{-1}$, and $2,971\text{ cm}^{-1}$ were attributed to the stretching vibration of the S=O bond, C-H bond, and C-O-C group, respectively (Kuvarega *et al.* 2018). It was simultaneously found that the S=O and C-O-C groups were present in the pristine and modified membrane, while the peak intensity of both gradually waned when the resin content increased.

In addition, a broad adsorption at about $3,455\text{ cm}^{-1}$ belongs to the stretching vibration of the –OH groups. It can be seen that the intensity of this adsorption increased significantly. This result was attributed to the hydrophilic resins and indicated successful incorporation of resin in the membrane matrix.

Membrane surface morphology

The surface and cross-section morphology of raw membrane and modified membranes were visualized using SEM and the images are shown in Figure 2. It can be seen that the pristine membrane presented a smooth and clean surface morphology, and the cross-sectional image revealed a typical finger-like pore structure. In contrast, the surface and cross-section morphology of modified membranes further emerged as heterogeneity, roughness and deformation became increasingly

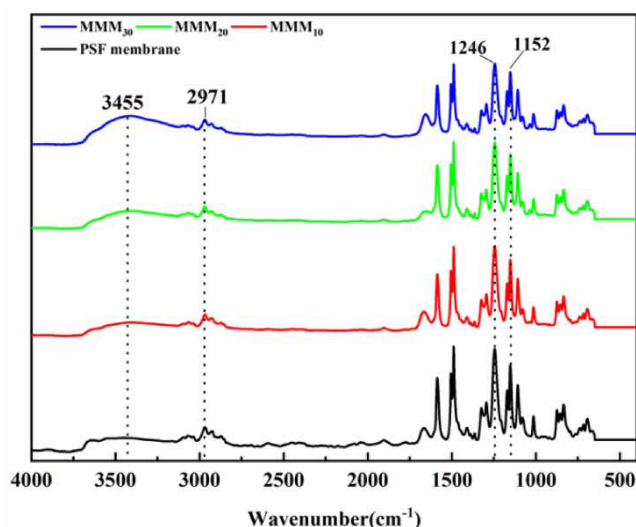


Figure 1 | FTIR spectra of the PSF, MMM_{10} , MMM_{20} and MMM_{30} .

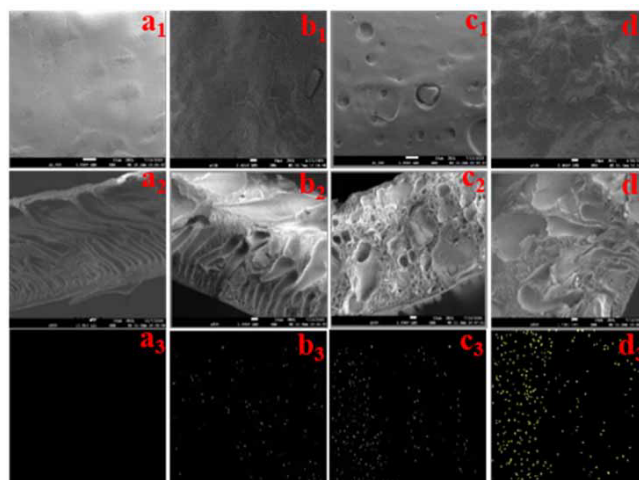


Figure 2 | SEM images of the surface and cross-section membranes, PSF (a₁, a₂, a₃), MMM₁₀ (b₁, b₂, b₃), MMM₂₀ (c₁, c₂, c₃) and MMM₃₀ (d₁, d₂, d₃) and EDS images showing the distribution of Al element (yellow point).

apparent with the increased dosage of resin. The addition of more resin led to the membrane producing sediment and agglomeration, which destroyed the membrane morphology during the phase inversion process. The presence of resin in the membranes was evaluated by EDS due to the presence of aluminum-based groups in the resin. As shown in Figure 2 and Table 1, the presence of Al element was not detected in the PSF membranes; however, significant Al element was detected in the modified membranes and increased with increasing resin content. This confirmed that the resin was successfully blended into the membrane. The resin migrated to the membrane's finger-like pore structure by the resin particle precipitation in the phase inversion process, and further changed the modified membrane cross-section morphology with addition of resin. Thus, the resin content should be controlled by the addition of 30 g to ensure the membrane structure remained stable. At the same time this contributed to improving the membrane adsorption capacity due to the introduction of more resin.

Adsorption isotherm

To elucidate the adsorption mechanism and further evaluate the adsorption capacity of MMM, the fitting adsorption isotherm was obtained and investigated in terms of the function of fluorine ion uptake (Q_e) and fluoride ion equilibrium concentration (C_e). In addition, the Langmuir, Freundlich, D-R and Redlich–Peterson models were used to describe and analyze the adsorption isotherm. The Langmuir isotherm model assumed that the monolayer adsorption on the adsorbent surface exhibited uniform energy. Meanwhile, the Freundlich isotherm model assumed the process of multilayer adsorption on the heterogeneous adsorbent surface. The D-R isotherm is more general than Langmuir isotherm because it does not assume a homogeneous surface or constant adsorption potential. Redlich–Peterson isotherm model describes both the features of Langmuir as well as Freundlich isotherm.

Figure 3(a) illustrates the adsorption isotherm models fitting results of the MMM with different amounts of resin content. It indicated that the isotherm curve of MMM presented gradually increased during the initial stages until the adsorption platform appeared. All the curves displayed a similar trend. The adsorption isotherm model parameters are shown in Table 2. It was further discovered according to the fitting results that the Langmuir model has a higher correlation coefficient (R^2) than

Table 1 | Analysis of element proportion on membrane surface

Elemental Percentage (%)	PSF	MMM ₁₀	MMM ₂₀	MMM ₃₀
C	26.79	26.53	26.66	25.78
O	72.47	72.49	72.30	71.82
S	0.74	0.67	0.6	1.67
Al	0	0.31	0.44	0.73

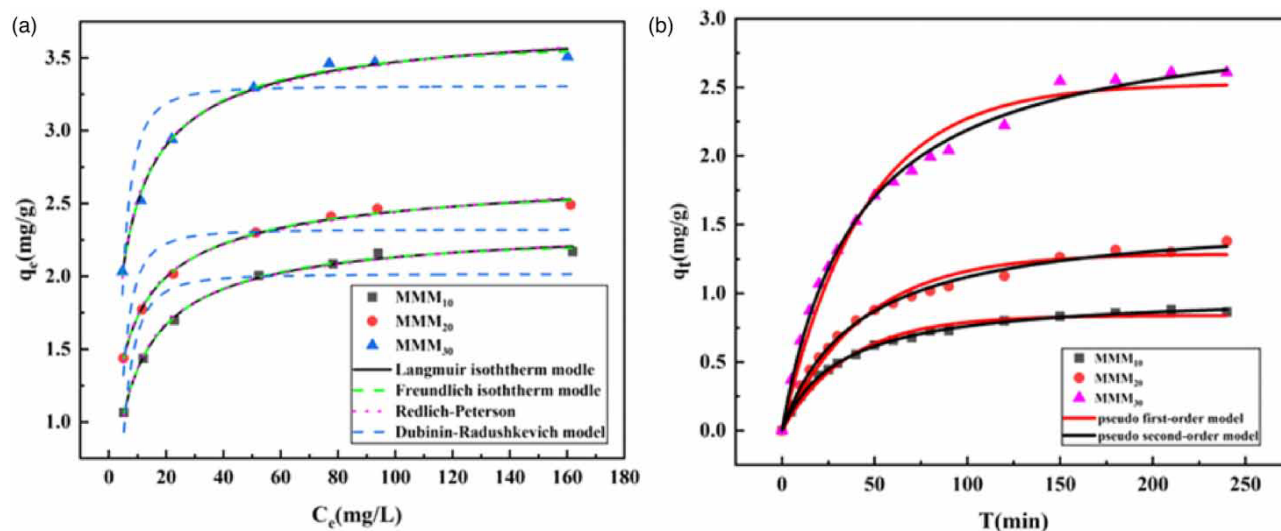


Figure 3 | (a) adsorption isotherm models of MMM₁₀, MMM₂₀, and MMM₃₀ for fluoride ion (pH = 6), (b) pseudo-first-order and pseudo-second-order of the MMM at the same initial fluoride ion concentration ($C_0 = 6$ mg/L, pH = 6).

Table 2 | Adsorption isotherm model parameters of MMM for fluoride ion

Sample		MMM ₁₀	MMM ₂₀	MMM ₃₀
Langmuir model	b(L/mg)	0.207	0.366	0.357
	q_m (mg/g)	2.380	2.795	3.808
	R^2	0.995	0.995	0.993
Freundlich model	1/n	0.188	0.152	0.146
	K_F	0.897	1.216	1.782
	R^2	0.912	0.937	0.910
Redlich–Peterson model	A	0.412	0.865	1.140
	B	0.220	0.461	0.388
	g	0.962	0.937	0.958
	R^2	0.991	0.989	0.987
D-R model	q_{DR} (mg/g)	2.017	2.320	3.306
	E(KJ/mol)	7.092	7.462	7.936
	R^2	0.780	0.742	0.771

other adsorption isotherm models, which is closer to the MMM adsorption of fluoride ion. And g of Redlich-Peterson model was calculated to be above 0.98, which concluded that the MMM has a strong affinity for fluoride ion. The high g-value confirms that adsorption of fluoride ion followed Langmuir model. It is suggested that the fluoride ion adsorption took place at the affinity sites of resin functional groups in the MMM and according to the characteristics of monolayer adsorption. However, the other isotherm models have similarly higher correlation coefficient values. Based on this, it appears that the adsorption of fluoride ion on the MMM uniform active site was not a simple adsorption process. In fact, a complex adsorption mechanism was involved in the adsorption process. It is noteworthy that the PSF membrane has no adsorption capacity for fluoride ions. Moreover, as can be seen from Table 2, the E values of all the adsorbents were below $8 \text{ kJ}\cdot\text{mol}^{-1}$, which suggests that it can be caused by the complexation reaction of fluoride selective groups in the resin with fluoride ions.

Adsorption kinetics

Figure 3(b) shows the effect of MMM adsorption fluoride ion capacity on contact time. Indicated here is that the fluoride ion adsorption rate increased rapidly in the first 100 min. Subsequently, the curves increased gradually and reached the adsorption equilibrium after 150 min. This phenomenon was explained by the MMM having more adsorption sites at the start which

led to the fluorine ion being easily adsorbed. The adsorption sites reduced in number gradually as time passed and the adsorption platform emerged.

Regarding MMM adsorption fluorine ion capacity, the kinetic models of the pseudo-first-order and pseudo-second-order were used to analyze the adsorption data. The relevant kinetic parameters are summarized and shown in Table 3. It can be seen that the pseudo-second-order model fitted better for the MMM adsorption kinetics with different amounts of resin compared with the pseudo-first-order model results. This was due to the higher correlation coefficient. In the meantime, the pseudo-second-order kinetic model revealed the adsorption rate was linked to two types of reactant concentration. Furthermore, the adsorption kinetic of MMM was influenced by the content of the hydroxy group and Al element. Then, the adsorption sites gradually decreased, which was brought about by fluorine ion adsorption difficulty.

To find out if the adsorption process limiting step has a diffusional or reactive nature, three models including chemisorption, intraparticle diffusion, and film diffusion were used to fit the results of adsorption kinetic data. The results are summarized in Table 4. The kinetic data of the chemisorption, intraparticle diffusion and membrane diffusion indicated that the adsorption process involved a multiple mixed mechanism. As the resin content in MMM increased, adsorption was mainly controlled by film diffusion, and low correlation coefficient (R^2) value indicated other diffusion was slightly affected. It can be inferred that fluorine ion diffused through the membrane to the outer surface of MMM for hydrogen bonding at the initial stage of adsorption. Then, the surface of MMM reached saturation, and fluorine ion may diffuse along the pore channels into the interior, and be adsorbed to the active groups of resin for complexation reaction. The adsorption of fluorine ion by MMM was complex and involved multiple processes. In this work, simple physical adsorption takes place, the rate of which is controlled by the diffusion layer on the membrane surface. The above results indicated that film diffusion was the rate-limiting step, which is in accordance with the structure of the MMM. Even though there were potential losses of the resin particulates in the phase inversion process, MMM still had higher competitive fluorine ion uptake compared with the pristine resin, on account of the increased accessibility of the Al group upon the milling process. It is known that the pore blockage due to the porosity in polymer resins can impede access of the complexing ligands with low uptake as a result (Mercier & Pinnavaia 1997). The buried ligands can be ‘recovered’ by milling the resin into finer particulates.

Effect of pH on adsorption of fluoride

In general, polysulfone membranes can be used in a pH range of 1–13. However, the pH value is one of the crucial factors in the adsorption process. Thus, the effect of pH on fluoride adsorption by MMM was investigated with an initial pH of solution varying from 4 to 10 (see Figure 4(a)). As shown in Figure 4(a), pH affected the fluoride adsorption capacity of MMM to some degree. The adsorption capacity of MMM increased with pH ranging from 4 to 6 and was afterwards reduced when pH was

Table 3 | Adsorption kinetics model parameters of MMM for fluorine ion

Sample	Pseudo-first-order model			Pseudo-second-order model		
	q_e (mg/g)	k_1 (min^{-1})	R^2	q_e (mg/g)	k_2 (g/mg·min)	R^2
MMM ₁₀	0.864	0.028	0.987	0.995	0.033	0.999
MMM ₂₀	1.379	0.023	0.981	1.567	0.160	0.996
MMM ₃₀	2.608	0.023	0.980	3.062	0.008	0.996

Table 4 | Diffusion model parameters of MMM for fluorine ion

Sample	Film diffusion model		Intraparticle diffusion model		Chemical reaction model	
	k_f	R^2	k_i	R^2	k_c	R^2
MMM ₁₀	0.028	0.987	0.070	0.855	0.006	0.949
MMM ₂₀	0.026	0.991	0.099	0.878	0.007	0.953
MMM ₃₀	0.027	0.989	0.194	0.876	0.006	0.930

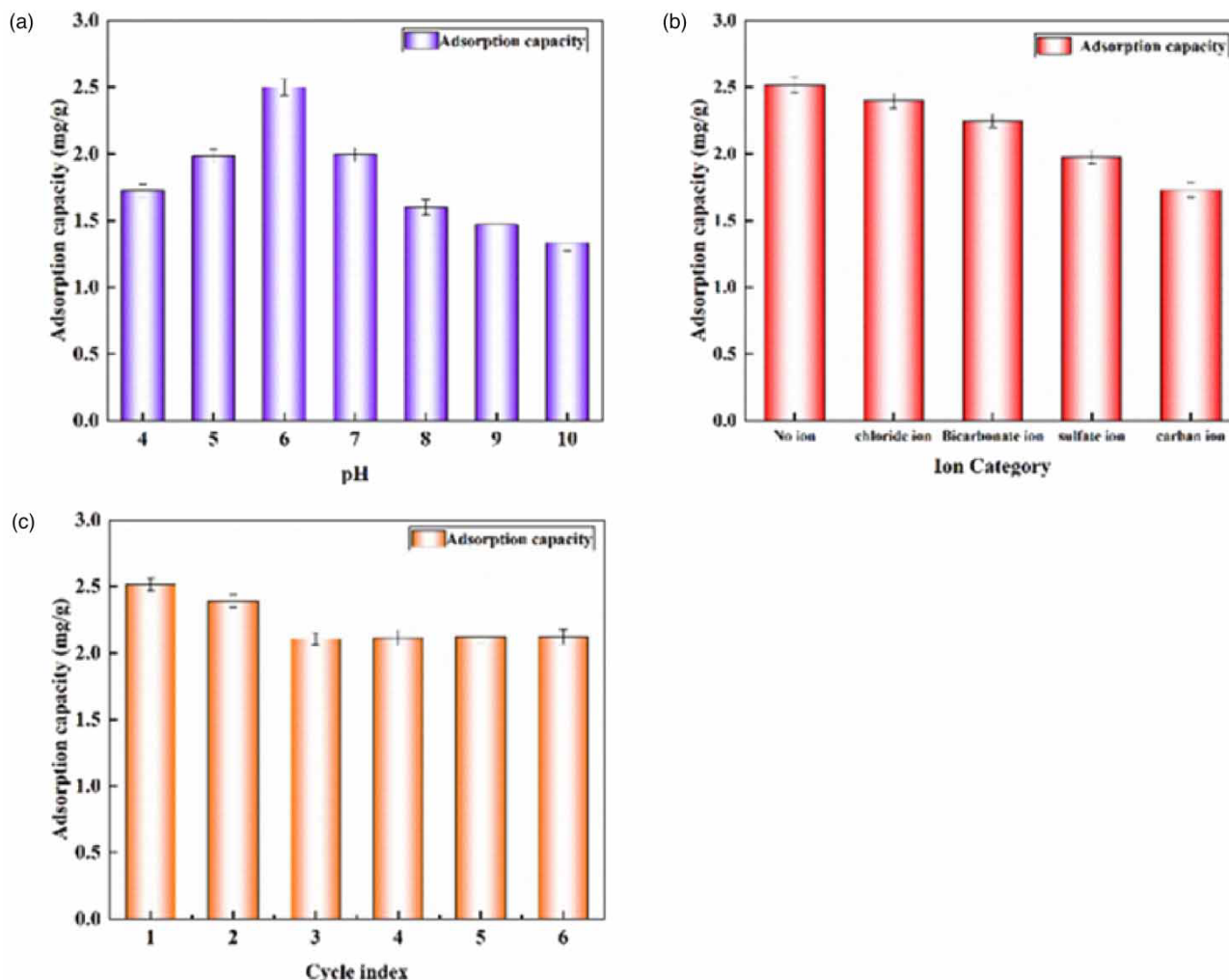


Figure 4 | (a) effect of pH on adsorption capacity of MMM₃₀ (C₀ = 6 mg/L), (b) effect of co-existing ions on the adsorption of fluorine ion on MMM₃₀ (C₀ = 6 mg/L, pH = 6), (c) cycled use of the MMM₃₀ (C₀ = 6 mg/L, pH = 6).

more than 6. The maximum adsorption capacity was 2.502 mg/g, which was presented at a pH of 6, and the solution pH is maintained around 6 before and after adsorption. The best pH value of MMM removal fluorine ion was in keeping with traditional. This result indicated that the OH⁻ ions displace fluorine ions from the surface of the sorbent, since OH⁻ ions interact very well with aluminum ions in the sorbent. Fluorine ions interacted with aluminum up to pH 6. However, OH⁻ ions in the solution became larger and they displaced fluorine ions from the surface of the sorbent at pH above 6. Consequently, the appropriate pH is 6 for fluoride adsorption.

Effect of co-existing anions

In fact, the various anions of inorganic salt are usually present in fluoride wastewater. Coexisting anions can compete with fluoride ions for active sites during the adsorption process and affect the removal performance of MMM (Goswami & Purkait 2014). The co-existing anions depended on affinity with MMM, which was intrinsically linked to the ion radius and charge amount (Tao *et al.* 2020). The effect of co-existing anions on MMM fluorine ion adsorption behavior was further studied individually by adding inorganic salts including Cl⁻, HCO₃⁻, CO₃²⁻ and SO₄²⁻ anions to the concentration of 0.1 mol/L at a pH of 6. The results for this are shown in Figure 4(b). It can be seen that the fluorine ion adsorption capacity of MMM fell away when adding anions of inorganic salt. The effectiveness of co-existing anions interference followed the sequence Cl⁻ < HCO₃⁻ < SO₄²⁻ < CO₃²⁻. The presence of the Cl⁻ and HCO₃⁻ monovalent anions revealed insignificant effects for the MMM adsorption fluorine ion. In contrast, the divalent anion yields a more significant influence on adsorption capacity.

This outcome for the co-existing anions effect is consistent with the anion charge/radius (nm, Z/r) values according to the following order: Cl^- (5.52) < HCO_3^- (6.41) < SO_4^{2-} (7.70) < CO_3^{2-} (11.23). The higher Z/r values lead to easy competition with fluorine ions to bond with the MMM. In addition, the anion Cl^- has the lowest Z/r value and relatively low-affinity ligand with weak bonds concerning outer-sphere complexation with the MMM active site. Consequently, the adsorption capacity of adding monovalent anions to the fluorine solution was better than that of divalent anions. It was made possible by the higher ion radius and charge amounts of divalent anions promoting the charge repulsion and steric hindrance effect. This replaced the fluorine ion on the MMM adsorption sites and led to a decline in the adsorbate adsorption efficiency.

Cycled use of the membrane

A regeneration experiment was conducted to evaluate the MMM reusability properties in the process of removing fluorine ion. The 10% aluminum sulfate solution functioned to desorb the fluorine ion on the MMM adsorption site and the six cycles result concerning adsorption-desorption is shown in Figure 4(c). It can be seen that the adsorption capacity of MMM declined after two regenerations, which may be caused by irreversible chemical adsorption. Subsequently, the regeneration efficiency remained above 80% after six recycling attempts, and this indicates the MMM has excellent and stable recyclability.

Adsorption mechanism

The analysis of SEM-EDS showed that MMM had a large amount of Al element (Figure 2), which was favorable for complexation. The removal of fluoride ions occurred on the surface of Al element, and Al complexed with F^- during the adsorption process, thus forming Al-F bonds. This played an important role in the fluoride adsorption process. In addition, the E values in the D-R model were all less than 8. Therefore, it was concluded that the fluorine ion was mainly removed by the combination of Al and fluorine to form a complex.

CONCLUSION

The MMM was successfully prepared by blending resin with polysulfone via phase inversion. SEM and FTIR characterization of the MMM showed that the resin particles were successfully embedded into the PSF. The adsorption capacity of fluorine ion gradually increased when more resin content was evident, and the maximum adsorption capacity was 2.502 mg/g with the initial antibiotic concentration of 6 mg/L and pH of 6. It is clear that MMM has a better adsorption capacity for fluoride and the regeneration effect is more stable. This study researched fluorine ion removal processes and the main mechanisms were complexation. Results showed that MMM combined the advantages of resins in terms of high absorption and membranes in terms of convective transport. Finally, this study demonstrated that MMM had the potential to serve as an effective adsorbent for fluoride removal from water. It represents a new technology that can be effective in rapid fluoride removal.

ACKNOWLEDGEMENT

The work was supported by Tianjin Municipal Science and Technology Bureau of China (No. 20JCYBJC00560), and TG Hilyte Environment Technology (Beijing) Co., LTD. (Project No. M-P-0-181001-001).

CONFLICT OF INTEREST STATEMENT

The authors declare that they have no known competing financial interests or personal relationships that could have appeared to influence the work reported in this paper.

DATA AVAILABILITY STATEMENT

All relevant data are included in the paper or its Supplementary Information.

REFERENCES

- Barbier, O., Arreola-Mendoza, L. & Del Razo, L. M. 2010 Molecular mechanisms of fluoride toxicity. *Chem. Biol. Interact.* **188** (2), 319–333.
- Cao, J., Chen, J., Wang, J., Jia, R., Xue, W., Luo, Y. & Gan, X. 2013 Effects of fluoride on liver apoptosis and Bcl-2, Bax protein expression in freshwater teleost *Cyprinus carpio*. *Chemosphere* **91** (8), 1203–1212.

- Dong, S. & Wang, Y. 2016 Characterization and adsorption properties of a lanthanum-loaded magnetic cationic hydrogel composite for fluoride removal. *Water Res.* **88**, 852–860.
- Dubinin, M. M., Zaverina, E. D. & Radushkevich, L. V. 1947 Sorption and structure of active carbons. I. Adsorption of organic vapors. *Zh.fiz.khim.* **21** (3), 151–162.
- Emamjomeh, M. M. & Sivakumar, M. 2009 Review of pollutants removed by electrocoagulation and electrocoagulation/flotation processes. *J. Environ. Manage.* **90** (5), 1663–1679.
- Goswami, A. & Purkait, M. K. 2014 Removal of fluoride from drinking water using nanomagnetite aggregated schwertmannite. *J. Water Process Eng.* **1**, 91–100.
- Grabow, W. O. K., Taylor, M. B. & De Villiers, J. C. 2001 New methods for the detection of viruses: call for review of drinking water quality guidelines. *Water Sci. Technol.* **43** (12), 1–8.
- Guillen, G. R., Pan, Y., Li, M. & Hoek, E. M. 2011 Preparation and characterization of membranes formed by nonsolvent induced phase separation: a review. *Ind. Eng. Chem. Res.* **50** (7), 3798–3817.
- Janssen, S., Schwahn, D., Mortensen, K. & Springer, T. 1993 Pressure dependence of the Flory-Huggins interaction parameter in polymer blends: a SANS study and a comparison to the Flory-Orwoll-Vrij equation of state. *Macromolecules* **26** (21), 5587–5591.
- Kuvarega, A. T., Khumalo, N., Dlamini, D. & Mamba, B. B. 2018 Polysulfone/N, Pd co-doped TiO₂ composite membranes for photocatalytic dye degradation. *Sep. Purif. Technol.* **191**, 122–133.
- Mercier, L. & Pinnavaia, T. J. 1997 Access in mesoporous materials: advantages of a uniform pore structure in the design of a heavy metal ion adsorbent for environmental remediation. *Adv. Mater.* **9** (6), 500–503.
- Owusu-Agyeman, I., Shen, J. & Schäfer A, I. 2018 Renewable energy powered membrane technology: impact of pH and ionic strength on fluoride and natural organic matter removal. *Sci. Total Environ.* **621**, 138–147.
- Paudyal, H., Pangen, B., Ghimire, K. N., Inoue, K., Ohto, K., Kawakita, H. & Alam, S. 2012 Adsorption behavior of orange waste gel for some rare earth ions and its application to the removal of fluoride from water. *Chem. Eng. J.* **195**, 289–296.
- Rana, D., Bag, K., Bhattacharyya, S. N. & Mandal, B. M. 2000 Miscibility of poly (styrene-co-butyl acrylate) with poly (ethyl methacrylate): existence of both UCST and LCST. *J. Polym. Sci. B Polym. Phys.* **38** (3), 369–375.
- Sarıcı-Özdemir, Ç. & Önal, Y. 2010 Equilibrium, kinetic and thermodynamic adsorptions of the environmental pollutant tannic acid onto activated carbon. *Desalination* **251** (1/3), 146–152.
- Shi, Q., Meng, J. Q., Xu, R. S., Du, X. L. & Zhang, Y. F. 2013 Synthesis of hydrophilic polysulfone membranes having antifouling and boron adsorption properties via blending with an amphiphilic graft glycopolymer. *J. Membr. Sci.* **444**, 50–59.
- Tao, W., Zhong, H., Pan, X., Wang, P., Wang, H. & Huang, L. 2020 Removal of fluoride from wastewater solution using Ce-ALOOH with oxalic acid as modification. *J. Hazard. Mater.* **384**, 121373.
- Wang, Z., Wang, P., Cao, J., Zhang, Y., Cheng, B. & Meng, J. 2017 A novel mixed matrix membrane allowing for flow-through removal of boron. *Chem. Eng. J.* **308**, 557–567.
- Wendimu, G., Zewge, F. & Mulugeta, E. 2017 Aluminium-iron-amended activated bamboo charcoal (AIAABC) for fluoride removal from aqueous solutions. *J. Water Process Eng.* **16**, 123–131.
- Zhao, S., Wang, Z., Wang, J., Yang, S. & Wang, S. 2011 PSf/PANI nanocomposite membrane prepared by in situ blending of PSf and PANI/NMP. *J. Membr. Sci.* **376** (1/2), 83–95.

First received 27 February 2022; accepted in revised form 16 May 2022. Available online 24 May 2022